JACS
JOURNAL OF THE AMERICAN CHEMICAL SOCIETY

pubs.acs.org/JACS

Article

Visible-Light-Driven Rotation of Molecular Motors in Discrete Supramolecular Metallacycles

Zhao-Tao Shi,[†] Yi-Xiong Hu,[†] Zhubin Hu, Qi Zhang, Shao-Yu Chen, Meng Chen, Jing-Jing Yu, Guang-Qiang Yin, Haitao Sun, Lin Xu, Xiaopeng Li, Ben L. Feringa,* Hai-Bo Yang,* He Tian, and Da-Hui Qu*

Cite This: *J. Am. Chem. Soc.* 2021, 143, 442−452

Read Online

ACCESS | Metrics & More | Article Recommendations | Supporting Information

ABSTRACT: The organization of molecular motors in supramolecular assemblies to allow the amplification and transmission of motion and collective action is an important step toward future responsive systems. Metal-coordination-driven directional self-assembly into supramolecular metallacycles provides a powerful strategy to position several motor units in larger structures with well-defined geometries. Herein, we present a pyridyl-modified molecular motor ligand (**MPY**) which upon coordination with geometrically distinct di-Pt(II) acceptors assembles into discrete metallacycles of different sizes and shapes. This coordination leads to a red-shift of the absorption bands of molecular motors, making these motorized metallacycles responsive to visible light. Photochemical and thermal isomerization experiments demonstrated that the light-driven rotation of the motors in the metallacycles is similar to that in free **MPY** in solution. CD studies show that the helicity inversions associated with each isomerization step in the rotary cycle are preserved. To explore collective motion, the trimeric motor-containing metallacycle was aggregated with heparin through multiple electrostatic interactions, to construct a multi-component hierarchical system. SEM, TEM, and DLS measurements revealed that the photo- and thermal-responsive molecular motor units enabled selective manipulation of the secondary supramolecular aggregation process without dissociating the primary metallacycle structures. These visible-light-responsive metallacycles, with intrinsic multiple rotary motors, offer prospects for cooperative operations, dynamic hierarchical self-assembled systems, and adaptive materials.

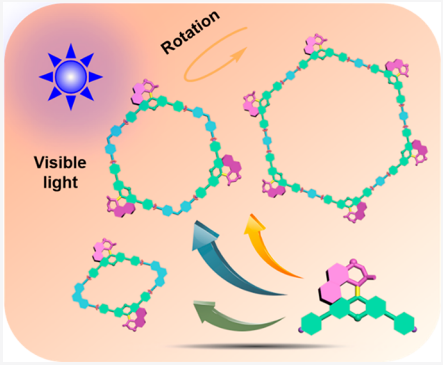

INTRODUCTION

Molecular machines are the key to nearly every essential process in living systems, ranging from fuel production to transport or muscle function, and normal cellular activities depend on various cooperative and collective motions of massive numbers of biomolecular motors.[1] Inspired by these intriguing processes and fascinating functions, a variety of man-made molecular machines have been successfully synthesized in the past decades,[2−13] several of which have shown intricate mechanical behavior and revealed potential applications in future responsive molecular systems and smart materials.[14−29] Overcrowded alkene-based molecular motors, a typical class of molecular machines, show intrinsic directional rotary motion driven by external light and heat stimuli.[30−32] To date, molecular motors have been widely employed in developing, e.g., dynamic materials for ion recognition,[33] asymmetric catalysis,[34,35] and chirality switching.[36,37] To mimic biomolecular motors enabling collective movements, molecular motors have been successfully incorporated into macroscopic materials, including liquid crystals,[38,39] glass or gold surfaces,[40−42] polymer gels,[43,44] muscle-like fibers,[45] and metal−organic frameworks.[46,47] However, most of these systems require complex pre-modifications to ensure collective operations of the molecular motors. Exploring simple and effective methods to organize several molecular motors is highly warranted. It will greatly facilitate those applications which critically rely on amplification and transmission mechanisms in multi-component dynamic systems.

As a result of one of the major developments in chemistry in the past decades, i.e., the coordination-driven directional self-assembly strategy, numerous novel supramolecular metal-coordination architectures ranging from two-dimensional (2-D) metallacycles to three-dimensional (3-D) metallacages with well-defined shapes, sizes, and geometries have been produced.[48−58] These supramolecular coordination complexes not only show astonishing geometrical structures but also enable a range of functions including supramolecular catalysis,[59−62]

Received: November 11, 2020
Published: December 28, 2020

https://dx.doi.org/10.1021/jacs.0c11752
J. Am. Chem. Soc. 2021, 143, 442−452

Scheme 1. Structures and Self-Assembly Process of Racemic Molecular Motor-Based Ligand MPY and with Di-Pt(II) Acceptors with Distinct Angles (60° for 2,120° for 3, and 180° for 4) to Give Different Size Metallacycles

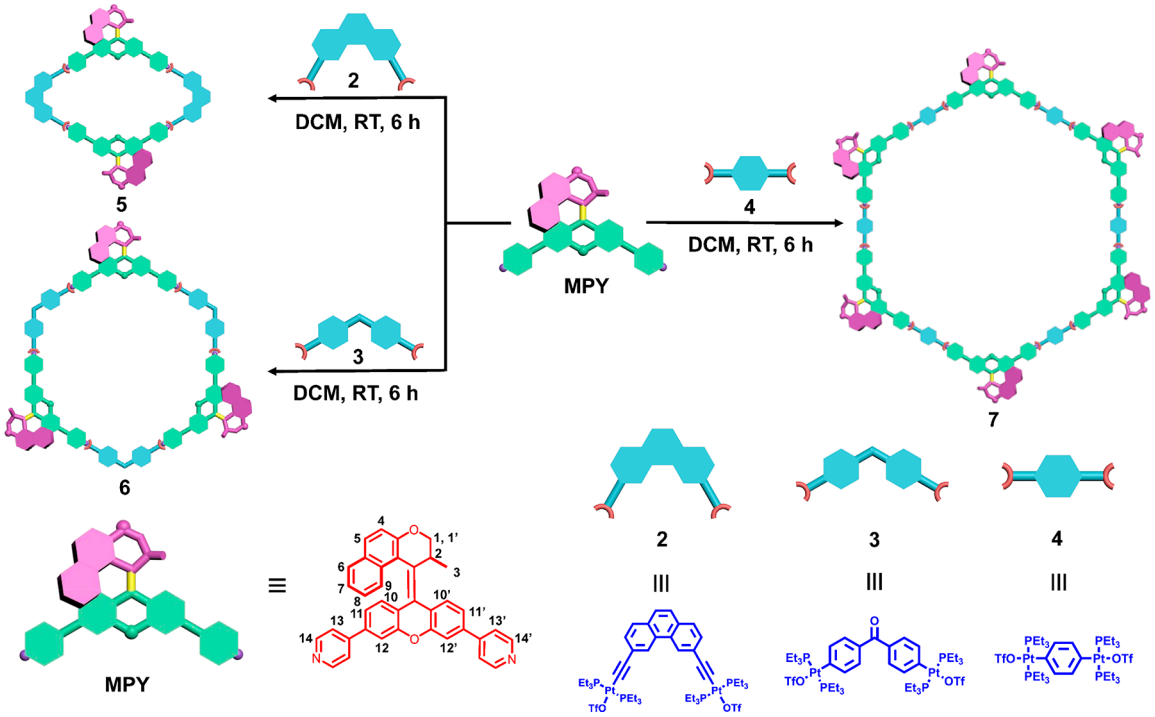

encapsulation,[63−67] liquid crystal,[68−72] control of optical properties,[73−76] and use in photodynamic therapy.[77−81] Due to the highly directional and comparatively strong metal−ligand bonds, the synthesis of self-assembled metallacycles and metallacages via the coordination of simple metal and ligand precursors is straightforward and nearly quantitative. Taking advantage of these robust and readily accessible self-assembled systems, a next level of design is focused on the introduction of responsive behavior. For example, Stang et al. pioneered photo-controlled transformations from discrete metallacycles to metallo-supramolecular polymers induced by *Z*- and *E*-configurational changes of embedded stiff stilbene units.[82] Other stimuli-responsive metal−ligand assemblies have been reported.[83−85] The fabrication of novel functional supramolecular metallacycles and metallacages, via the coordination-driven self-assembly strategy, featuring intrinsic responsive functions, offers fascinating opportunities to achieve cooperative action, adaptive organization, and responsive material properties.

Toward this goal, we designed a bis-pyridyl-based molecular motor ligand, **MPY** (Scheme 1). The precise geometry of the electron-rich **MPY** donor moieties allow them to coordinate with different electron-deficient di-Pt(II) acceptors **2**−**4** to form discrete metallacycles. Several design features need to be emphasized. First, we anticipate that due to sufficient free volume in the metallo-supramolecular structures, the photoisomerization and THI of molecular motors located on the macrocycles are not restricted by the coordination topologies, allowing for not only the transformation of molecular geometry but also the chirality of self-assembled metallacycles. In addition, compared to the free ligand, coordinating the **MPY** with the di-Pt(II) acceptors results in an electron density shift toward the acceptor units. As a consequence, new push−pull systems involving the rotor and stator of molecular motors are established, accompanied by a red-shift of the absorption wavelength and an increase of the molar absorption coefficient for the motors, which potentially enables these metallacycles to be driven by visible light. Finally, taking advantages of the positive charges and stimuli-responsiveness of the metallacycles, the initially formed metallacycles were employed to further aggregate with negatively charged heparin to form cross-linked networks, in which the materials could transform into discrete assemblies when the stable motor isomers switch to metastable isomers triggered by visible light (420 nm) without destroying the primary nanospheres' or linear aggregates' structures. We reasoned that this coordination-driven self-assembly could present a new strategy of organizing molecular motors to exploit their cooperative and collective motions. Meanwhile, as an additional benefit, these visible-light-responsive metallacycles may exhibit potential for future biocompatible smart materials.

RESULTS AND DISCUSSION

Synthesis and Characterization. The structures of motor **MPY** bearing two pyridine ligands in the stator part and Pt-complexes **2**−**4**[86−88] are depicted in Scheme 1. The synthesis route toward photo- and thermal-responsive molecular-motor-based ligand **MPY** is shown in Scheme S1. First, compound **1** was synthesized as described previously.[89] Subsequently, the desired ligand **MPY** was obtained by a double Suzuki coupling between compound **1** and 4-pyridineboronic acid pinacol ester in 76% yield. The structure of **MPY** was confirmed using ^{1}H NMR and ^{13}C NMR spectroscopy and high-resolution electronic spray ionization (HR-ESI) mass spectrometry (detailed information given in the Supporting Information). NMR absorption signals were fully assigned by ^{1}H−^{1}H COSY, HMBC, and HMQC analysis (Figure S1).

The single-crystal structure of racemic **MPY** revealed that the angle between its two pyridyl sites was approximately 110° (Figure S2 and Table S1). Guided by the directional-bonding approach,[48] the racemic metallacycles, i.e., rhomboid **5**, [3+3]

https://dx.doi.org/10.1021/jacs.0c11752
J. Am. Chem. Soc. 2021, 143, 442−452

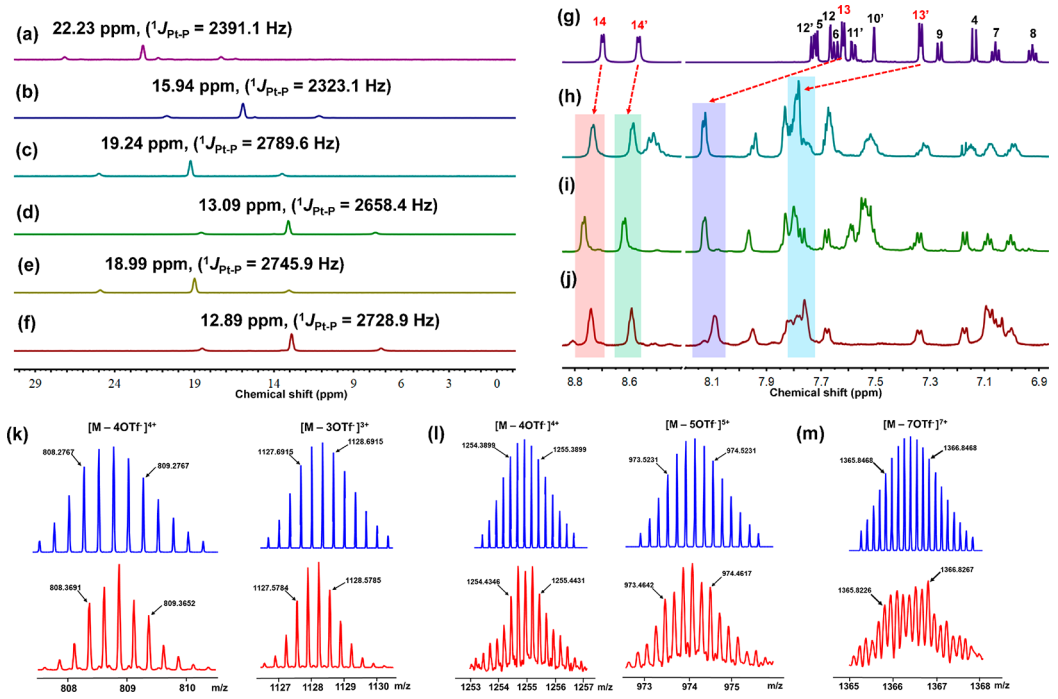

Figure 1. ^{31}P NMR spectra (243 MHz, CD_2Cl_2, 298 K) of 60° acceptor **2** (a), rhomboid **5** (b), 120° acceptor **3** (c), hexagon **6** (d) 180° acceptor **4** (e), and hexagon **7** (f). Partial ^{1}H NMR spectra (600 M, CD_2Cl_2, 298 K) of **MPY** (g), rhomboid **5** (h), hexagon **6** (i), and hexagon **7** (j). For the proton assignment, see Scheme 1. Theoretical (*top*) and experimental (*bottom*) ESI-TOF-MS of rhomboid **5** (k), hexagon **6** (l), and hexagon **7** (m).

hexagon **6**, and [6+6] hexagon **7**, were obtained quantitatively by stirring a mixture of **MPY** and di-Pt(II) acceptors **2**, **3**, and **4** at a 1:1 molar ratio in CH_2Cl_2, respectively (Scheme 1). Multinuclear NMR spectroscopy was used to confirm the structure of new metallacycles. For instance, the ^{31}P{^{1}H} NMR spectra of metallacycles **5**−**7** exhibited sharp singlets (ca. 15.94 ppm for **5**, 13.09 ppm for **6**, and 12.89 ppm for **7**) shifted upfield by approximately 6.29, 6.15, and 6.10 ppm, relative to the starting platinum acceptors **2**, **3**, and **4**, respectively. This upfield shift, along with a decreased coupling of flanking ^{195}Pt satellites (ca. ΔJ_{PPt} = −68.0 Hz for **5**, ΔJ_{PPt} = −131.2 Hz for **6**, ΔJ_{PPt} = −17.0 Hz for **7**), is consistent with back-donation from the platinum atoms (Figure 1a−f).[68,70]

The structures of the metallacycles were further studied by ^{1}H NMR spectroscopy. Compared to the proton signals of the pyridyl moieties in the free ligand **MPY** (Figure 1g), downfield shifts were observed in the spectrum of rhomboid **5** (Figure 1h) due to the loss of electron density upon the coordination of Pt and N atoms (ca. $\Delta\delta$ = 0.03 ppm for H_{14}, $\Delta\delta$ = 0.02 ppm for $H_{14'}$, $\Delta\delta$ = 0.51 ppm for H_{13}, $\Delta\delta$ = 0.45 ppm for $H_{13'}$). Similar changes were observed for metallacycles **6** and **7** (Figure 1i,j). The clear spectra and distinctive NMR signals in the ^{31}P, ^{1}H, and 2D NMR spectra (^{1}H−^{1}H COSY and DOSY) support the formation of discrete metallacycles (Figures S3−S11).

Electrospray ionization time-of-flight mass spectrometry (ESI-TOF-MS) analysis provided further evidence for the formation of discrete metallacycles. For example, the mass spectrum of rhomboid **5** revealed two peaks at m/z = 809.36 and m/z = 1128.57 (Figure 1k), corresponding to the different charge states as a result of losing counterions $[M-4OTf^-]^{4+}$ and $[M-3OTf^-]^{3+}$, respectively, where M represents the intact metallacycle. Meanwhile, the isotopic pattern of each peak was in good agreement with the theoretical distribution, indicating the existence of discrete rhomboid **5**. Additionally, the assigned peaks of hexagons **6** and **7** were also in accordance with their theoretical distributions (Figure 1l,m), confirming the formation of hexagon metallacycles.

Molecular simulations were performed to gain further insight into the spatial structure of the coordination complexes, as we were unable to obtain single crystals of the metallacycles even after repeated attempts. After simplifying the molecules by replacing the ethyl groups with methyl groups, the geometries of the metallacycles were optimized using the GFN2-xTB semiempirical tight-binding method with an implicit GBSA solvation model (dichloromethane).[90] As shown in Figure S12, the calculated geometries of these metallacycles featured well-defined cyclic structures with different-sized cavities. The changes of relative energy as a function of the rotation of naphthalene-based rotor for **MPY** and **5** are shown in Figure S13. The results indicate that the intermediate conformers with the naphthalene group almost perpendicular to the stator backbone are disfavored because of steric hindrance, which is in line with our recent findings.[91] The combined experimental data and theoretical simulations support the formation of metallacycle architectures.

UV−Vis Absorption Spectroscopy. UV−vis absorption spectra of the free ligand **MPY** and the metallacycles (Figure 2) showed that the ligand **MPY** displayed a characteristic absorption maximum at 370 nm with a molar absorption coefficient (ε) of 1.30 × 10^4 M^{-1} cm^{-1}. Interestingly, after forming discrete metallacycles, the absorption maximum of **MPY** exhibited a red-shift to 410 nm with an increase of the molar absorption coefficient to 1.40 × 10^4 M^{-1} cm^{-1}, indicating the change in optical properties of molecular motors in the metallacycles.

The observed bathochromic shift might be attributed to a new push−pull system formed between the upper half and lower half of the molecular motor upon Pt-coordination of the two pyridyl units of **MPY**. To verify our hypothesis, *N*-methylated reference compound **R** was prepared by using **MPY** and methyl iodide

https://dx.doi.org/10.1021/jacs.0c11752
J. Am. Chem. Soc. 2021, 143, 442−452

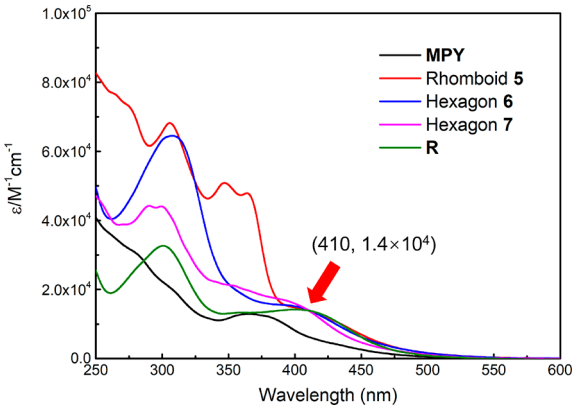

Figure 2. UV−vis absorption spectra of the free ligand **MPY**, discrete metallacycles (CH_2Cl_2, 298 K, $c = 1 \times 10^{-5}$ M), and the *N*-methylated reference compound **R** (CH_3CN, 298 K, $c = 1 \times 10^{-5}$ M). The molar extinction coefficients of the metallacycles are calculated based on the concentration of molecular motors.

(Figure 3a and Scheme S5). The UV−vis absorption spectra of **R** also exhibited a maximum at 410 nm with a molar absorption

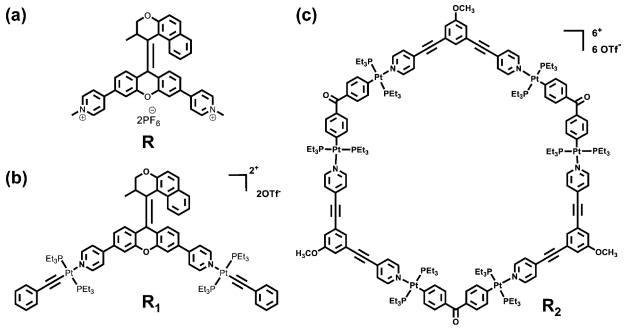

Figure 3. Structural formulas of reference compounds: (a) *N*-methylated compound **R**; (b) non-cyclic di-Pt(II) modified compound $\mathbf{R_1}$; and (c) non-light-responsive trimeric metallacycle $\mathbf{R_2}$.

coefficient of 1.40×10^4 M^{-1} cm^{-1} (Figure 2, green line). Theoretical simulations were used to provide further support for this explanation. Compared with the free ligand **MPY**, the calculated HOMO→LUMO gap for compound **5** is reduced from 5.34 to 4.49 eV (Figure S14), indicating that the formation of the metallacycle will result in a red-shift of the maximum wavelength for the molecular motor unit, which is in consistent with the experimental results. Furthermore, hole−electron analysis of the lowest singlet (S_1) excited states for **MPY** and metallacycles **5** was also performed (Figure S15). The metallacycle **5** possesses relatively smaller hole−electron wave function overlap (S_r) and larger distance between the centroids of the hole and electron distributions (D) than **MPY**, indicating a stronger charge-transfer excitation of the metallacycle **5** resulting from the coordination of N and Pt atoms. Meanwhile, we also showed that the reference compound **R** can undergo efficient photo- and thermal isomerization steps upon exposure to light (420 nm) and heat (Figure S16), which indicates that the motor units in these metallacycles might be driven by visible light.[92−96]

Photochemical and Thermal Isomerization of MPY and Metallacycles. The light- and thermally induced isomerization processes of motor **MPY** and metallacycles **5**−**7** were analyzed using UV−vis absorption spectroscopy. A diluted dichloromethane solution of free ligand **MPY** showed a strong absorption band at 340−390 nm in the UV−vis spectrum. New red-shift absorption bands appear between 390 and 550 nm with clean isosbestic points at 345 and 390 nm upon irradiation with 365 nm light for 90 s at −20 °C (Figure 4a), indicating the

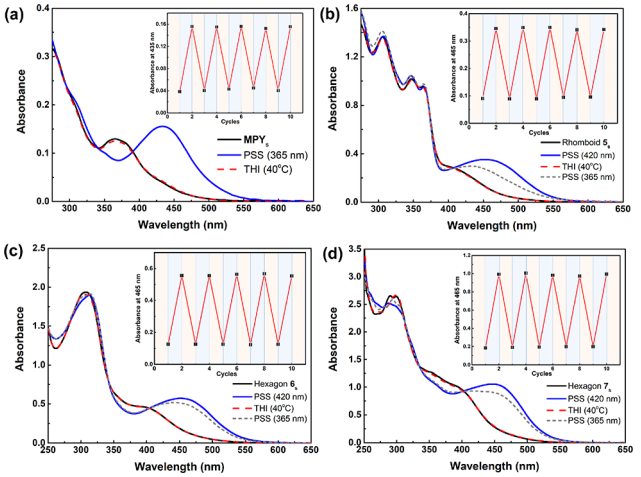

Figure 4. UV−vis absorption spectra (CH_2Cl_2, $c = 1 \times 10^{-5}$ M) of **MPY** and metallacycles before/after photo- and thermal isomerization: (a) **MPY**, (b) rhomboid **5**, (c) hexagon **6**, and (d) hexagon **7**. The insets show the change in UV−vis absorption at 435 nm for **MPY** and 465 nm for metallacycles after several irradiation/heating cycles.

formation of the metastable isomers. A red-shifted absorption band is observed in the metallacycles **5**−**7**, indicating the possibility to trigger **5**−**7** with visible light. Two wavelengths of light (365 and 420 nm) were employed to irradiate the samples of **5**−**7** at −20 °C. The absorption spectra of metallacycles **5**−**7** displayed new red-shifted bands with clean isosbestic points (Figure 4b−d), confirming the successful photo-isomerization with both UV and visible light. Notably, the ratio of metastable isomers at PSS (420 nm) was higher than that at PSS (365 nm). To verify the subsequent thermal helix inversion (THI) process, the irradiated solutions of both **MPY** and metallacycles **5**−**7** were heated for 3 min at 40 °C, allowing the metastable isomers to undergo complete THI. Considering the symmetrical stator of **MPY**, the formed THI isomers were equivalent to the initial **MPY**. Therefore, the UV−vis spectra fully recovered to initial spectra after the THI process. Importantly, both free **MPY** and metallacycles show excellent fatigue resistance during the irradiation/heating processes, which could be repeated through multiple cycles without any degradation (Figure 4, insets), supporting the high stability and selectivity in multiple isomerizations.

The photo- and thermal isomerization processes were further confirmed by ^{1}H NMR analysis. As shown in Figure 5a and Figure S17, free ligand **MPY** in dichloromethane-d_2 showed distinctive proton shifts (ca. $\Delta\delta = -0.82$ ppm for H_1, $\Delta\delta = -0.51$ ppm for $H_{1'}$, $\Delta\delta = -0.37$ ppm for H_2, $\Delta\delta = 0.68$ ppm for H_3) in the ^{1}H NMR spectra upon exposure to UV light (365 nm) at −40 °C for 6 h with a metastable:stable isomer ratio of 78:22 at the PSS. The subsequent THI step was performed at 40 °C for 3 min along with the recovery of proton peaks of H_1, $H_{1'}$, H_2, and H_3, indicating the isomerization process of metastable isomers to stable isomers. Similar changes were also observed in the ^{1}H NMR spectra of the three different metallacycles **5**−**7** using visible-light (420 nm, 6 h)-driven photo-isomerization

https://dx.doi.org/10.1021/jacs.0c11752
J. Am. Chem. Soc. 2021, 143, 442−452

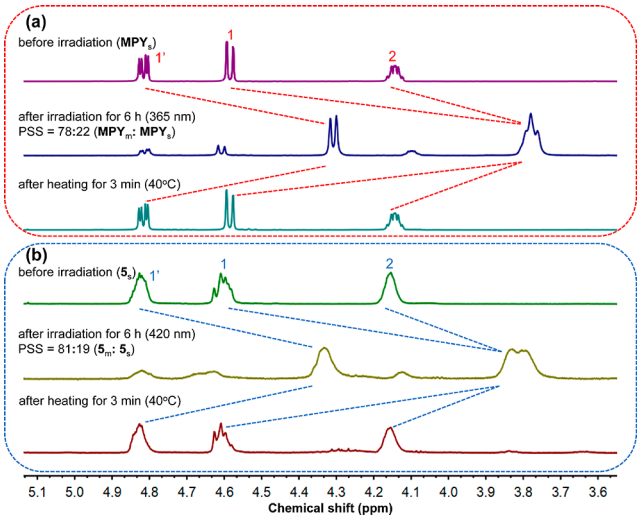

Figure 5. Partial ^{1}H NMR spectra of (a) free ligand **MPY** (600 MHz, CD_2Cl_2, −40 °C) before irradiation, at PSS, and after completed THI and (b) metallacycle **5** (600 MHz, CD_2Cl_2, −40 °C) before irradiation, at PSS, and after completed THI (**MPY**$_s$/**5**$_s$: stable isomer, **MPY**$_m$/**5**$_m$: metastable isomer).

(ratios of metastable:stable isomers at PSS are 81:19 for **5**, 73:27 for **6**, and 71:29 for **7**) and thermal isomerization (40 °C, 3 min) (Figure 5b and Figures S18−S20). The combination of UV−vis absorption and NMR analysis confirmed that (i) the metallacycles were capable of undergoing efficient photo- and thermal isomerization steps like the free **MPY**; (ii) the formation of the metallacycles **5**−**7** did not restrict the rotary motion of the molecular motors; and (iii) the unique visible-light-driven motion as well as excellent fatigue resistant make these metallacycles promising candidates for fabricating novel stimuli-responsive materials.

To investigate how the assembly into metallacycles affects the rotation speed of molecular motors, the thermal isomerization kinetics from metastable isomers to stable species were determined from UV−vis spectra at varied temperatures. The Gibbs free energy of activation (ΔG°) and corresponding half-life ($t_{1/2}$) of metastable isomers at 20 °C were obtained by using Eyring analysis (Table 1 and Figure S21). Based on the data in Table 1, the Gibbs free energy and half-life of the metastable metallacycles were comparable with those of the metastable free ligand, confirming that the formation of supramolecular metallacycles had no significant effect on the rotation speed of the molecular motors. The experimental and theoretical results indicate that the photo- and thermal isomerizations of motors in the metallacycles are independent of each other and no significantly synergistic or inhibitory effects are observed.

Table 1. Thermodynamic Parameters of Metastable Isomers for Thermal Helix Inversion of Free Ligand and Metallacycles as Determined by Eyring Analysis

compound	half-life at 20 °C (s)	ΔG° (kJ/mol)
MPY$_m$	55.7	82.5 ± 0.4
5$_m$	48.0	82.1 ± 1.3
6$_m$	50.8	82.2 ± 4.3
7$_m$	45.8	82.0 ± 2.4

Dynamic Chirality. Due to the unique molecular structure, the molecular motor has two distinguishable chiral elements: the methyl-substituted carbon stereogenic center (*R* or *S*) and the molecular helicity (*P* or *M*) induced by overcrowded double bond. Chirality can be used as a distinguishing feature to follow isomerization processes. In order to investigate the chiroptical properties, including change in isomerization of the free ligand **MPY** and metallacycles **5**−**7**, optically pure enantiomers (*S*,*P*)-**MPY** and (*R*,*M*)-**MPY** were isolated by using chiral HPLC (Figures S22−S24). The structure of enantiopure **MPY** was confirmed by single-crystal X-ray diffraction analysis (Figure S25 and Table S1), and the absolute configuration was determined by CD spectroscopy supported by calculations[91] (see Figure 6b and Figures S34 and S35). Subsequently, the chiral metallacycles were prepared by using enantiopure ligands to coordinate with di-Pt(II) acceptors **2**−**4**. No notable differences were observed in the ^{1}H NMR spectra of the metallacycles assembled by racemic or enantiopure motors, indicating the chirality had no impact on the coordination process (Figures S26−S29). Upon irradiation by UV light (365 nm), the stable (*S*,*P*)-**MPY** and (*R*,*M*)-**MPY** transformed into metastable isomers (*S*,*M*)-**MPY** and (*R*,*P*)-**MPY**, respectively, by photo-isomerization. Meanwhile, starting from the stable isomers with the methyl substituent at the stereogenic center in a pseudo-axial orientation, upon photo-isomerization the methyl substituent adopts a pseudo-equatorial orientation, in which conformational change accompanies the helix inversion. Subsequently, to release the steric strain of the structure, the metastable isomers thermally transform into the stable isomers by a unidirectional helix inversion process (Figures S30 and S31). We envisioned that the chirality of the molecular motors would display a collective enhancement and that similar helix transformations operate after forming the metallacycles (Figure 6a and Figure S32).

Circular dichroism (CD) spectroscopy was employed to monitor dynamic chirality associated with the helix inversion processes of the enantiomers of free ligand **MPY** and the metallacycles. As shown in Figure S33, the CD signals of the chiral metallacycles show quantitative enhancement compared to those of the chiral free ligand, attributed to an increased number of helical molecular motor units. The helicity inversion process of the free ligand (*S*, *P*)-**MPY** was monitored by CD spectroscopy (Figure 6b). Upon exposure of the solution to UV irradiation (365 nm) for 90 s, the CD spectra showed a distinct change with two isosbestic points at 274 and 362 nm, indicating the selective photo-isomerization step along with helicity inversion from (*S*,*P*)-**MPY** to (*S*,*M*)-**MPY**. The solutions obtained after irradiation were then heated at 40 °C for 3 min to induce the THI inversion of the metastable isomer (*S*,*M*)-**MPY**. The complete recovery of the original CD spectrum confirmed the helix inversion from (*S*,*M*)-**MPY** to (*S*,*P*)-**MPY**. CD measurements of the photochemical and thermal isomerizations of the enantiomeric free ligand (*R*,*M*)-**MPY** showed similar helix inversion steps, as evident from completely opposite changes in CD absorption (Figure 6b). Additionally, TDDFT calculations at the sTD-CAM-B3LYP/TZVP level reasonably reproduced the experimental CD spectra, further supporting the absolute stereochemical assignment of the isolated isomers and confirming the helicity inversion processes (Figure S34). To confirm whether the switching of helicity remained in the metallacycles, chiral rhombic metallacycles (*S*,*P*)-**5** and (*R*,*M*)-**5** were initially selected to study by CD the interconverting chirality during the photo- and thermal isomerization processes. As shown in Figure 6c, after irradiation with 420 nm light for 90 s, several isosbestic points at 244, 306, 334, and 370 nm in the CD spectra were observed, indicating

https://dx.doi.org/10.1021/jacs.0c11752
J. Am. Chem. Soc. 2021, 143, 442−452

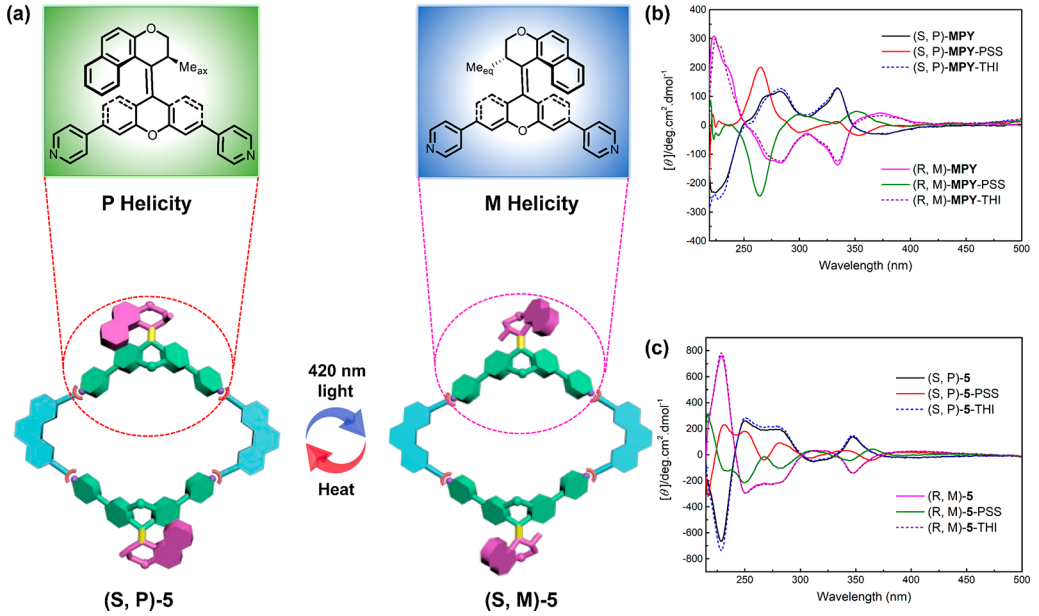

Figure 6. (a) Schematic illustration of photo- and thermal isomerization steps of chiral metallacycles (*S*,*P*)-**5** and (*S*,*M*)-**5**. (b) CD spectra changes of free ligands (*S*,*P*)-**MPY** and (*R*,*M*)-**MPY** upon photo- and thermal isomerization (CH_2Cl_2, $c = 5 \times 10^{-5}$ M, −20 °C). (c) CD spectra changes of metallacycles (*S*,*P*)-**5** and (*R*,*M*)-**5** upon photo- and thermal isomerization (CH_2Cl_2, $c = 5 \times 10^{-5}$ M, −20 °C).

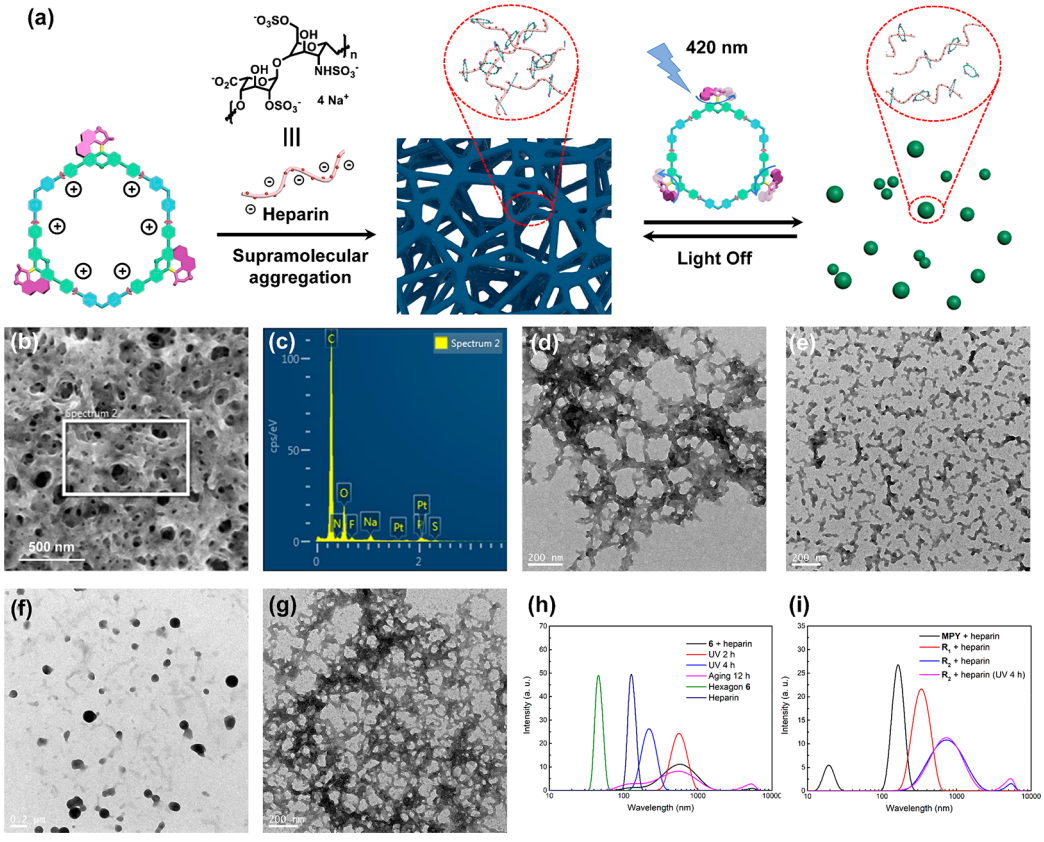

Figure 7. Schematic representation of the manipulated supramolecular aggregation of metallacycle **6** and heparin (a). SEM images of **6** and heparin composites (b). EDX results of **6** and heparin composites collected from the area marked by the white boxes (c). TEM images of **6** and heparin composites before 420 nm irradiation (d), after 420 nm irradiation for 2 h (e), after 420 nm irradiation for 4 h (f), and after 420 nm light irradiation for 4 h and continuous aging for 12 h (g). DLS data of **6** and heparin composites in the photo- and thermal isomerization steps (h). DLS data of referential composites formed by heparin with **MPY** and reference compound (i) in a mixture of acetone/water (3/7, v/v).

these two chiral metallacycles undergo selective photo-isomerization without any degradation. The changes in CD spectra indicated that the helicity in metallacycles has been reversed. Similar to the chiral free ligand, the original CD spectrum of (*S*,*P*)-**5** was fully recovered after the subsequent THI step. These helicity inversion steps were also supported by calculation

https://dx.doi.org/10.1021/jacs.0c11752
J. Am. Chem. Soc. 2021, 143, 442−452

of the CD absorptions (Figure S35). In addition, the enantiomers of chiral hexagonal metallacycles (*S*,*P*)-**6**, (*R*,*M*)-**6**, (*S*,*P*)-**7**, and (*R*,*M*)-**7** also displayed changes in the CD spectra similar to those shown for the chiral free ligand and rhombic metallacycle **5** (Figures S36 and S37), confirming that the motor units in the enantiomerically pure hexagonal metallacycles also undergo the normal helix inversion steps. These results demonstrated that, along with synergistic enhancement of the CD signals, effective isomerization and helicity inversion processes still operate in the molecular motor units of these chiral metallacycles.

Photochemically and Thermally Regulated Reversible Supramolecular Aggregation. Upon coordination of electron-rich **MPY** and electron-deficient di-Pt(II) acceptors, the formed metallacycles skeletons exhibited positive charges, endowing these metallacycles with the ability to undergo additional supramolecular aggregation with negative-charged compounds.[68,97] Furthermore, the photo- and thermal-responsive molecular motor units might render the system responsive to allow non-invasive control of such hierarchical aggregation (Figure 7a). To address this issue of regulating reversible self-assembly at the next hierarchical level, the trimeric metallacycle **6** was selected to bind to negative-charged heparin. Considering that heparin is insoluble in organic solvents, the morphologies of the aggregates and polymers and the subsequent stimuli-responsive behavior were investigated in a mixture of acetone/water (3/7, v/v). Scanning electron microscopy (SEM) and transmission electron microscopy (TEM) were used to study the size and morphologies of the supramolecular aggregates. In the solution of heparin (10 μM), dispersed nanospheres and linear aggregates were observed (Figure S38a). Notably, after addition of heparin (10 μg) to the solution of metallacycle **6** (10 μM), SEM and TEM experiments revealed that cross-linked networks were formed (Figure 7b,d). The formation of such aggregates is attributed to the electrostatic-interactions-induced supramolecular aggregation between positive-charged metallacycles and the negative-charged primary nanospheres and linear aggregates of heparin. Energy-dispersive X-ray spectroscopy (EDX) was employed to further investigate the components of the three-dimensional (3-D) network, confirming the elemental compositions comprising carbon, oxygen, nitrogen, platinum, fluorine, sulfur, and phosphorus (Figure 7c). The results provided strong support for the multi-component aggregates obtained. Furthermore, control experiments were performed to further confirm the aggregation process shown in Figure 7a. When heparin (10 μg) was added to a diluted solution of **MPY** (30 μM), TEM measurement revealed that only nanospheres and linear supramolecular polymers were formed (Figure S38b). In a control experiment, non-cyclic di-Pt(II)-modified reference compound $\mathbf{R}_1$ (Scheme S6) only resulted in the formation of non-cross-linked aggregates (Figure S38c−e), indicating the distinctive role of multi-charged metallacyclic structures in aggregating the negative-charged polymers into networks.

Next the question was addressed to what extent the light-driven rotation of molecular motors in the metallacycles could deliver responsiveness toward the cross-linked polymer network. A solution of metallacycle **6** (10 μM) with 10 μg of heparin was aged for 1 h to form the cross-linked aggregates and then exposed to 420 nm light for 2 h. TEM images showed that the cross-linked networks transformed into dispersed lamellar polymers (Figure 7e). Further irradiation made the lamellar aggregates transform into linked or dispersed nanospheres (Figure 7f). The transformations from 3-D networks to dispersed aggregates might be attributed to disruption of electrostatic interactions between motorized metallacycles and polymers by light-driven isomerization of molecular motors, wherein the influence of possible heating effects can be excluded by the control experiments (Figure S38f,g). After aging these irradiated solutions at room temperature for 12 h, the molecular motor units underwent a thermal isomerization step to regain their initial configurations, and as a consequence the original morphologies were obtained (Figure 7g and Figure S39). It should be emphasized that during the entire sequence of isomerization processes, the photo- and thermal-responsive molecular motor units seem to selectively affect the reversible secondary supramolecular aggregation process without destroying the primary aggregates. Additionally, a trimeric metallacycle reference compound $\mathbf{R}_2$ (Figure 3c and Scheme S7), without photo-responsive unit, was synthesized for further comparison. After heparin (10 μg) was added into the solution of $\mathbf{R}_2$ (10 μM), cross-linked networks were also observed (Figure S40a). However, these networks exhibited no notable changes after irradiation (420 nm) for 4 h (Figure S40b), suggesting that the photo-responsive morphological changes were attributed to the photo-isomerization motion of molecular motors (Figures S38c,d and S40).

Dynamic light scattering (DLS) experiments were performed to further investigate the statistic distribution of the aggregates and the photochemically induced changes. As shown in Figure 7h, the solutions of heparin (10 μM) and metallacycle **6** (10 μM) displayed uniform distributions with an average size of 125 and 45 nm, respectively. Upon addition of heparin (10 μg) into the solution of metallacycle **6** (10 μM), large supramolecular aggregates were formed, and the DLS curve displayed broad distributions with an average size of 615 nm, showing the formation of cross-linked networks. Importantly, after irradiation with 420 nm light for 2 h, the DLS curve displayed a distribution with an average size of 550 nm, and continuous irradiation (4 h) resulted in a smaller average size of 220 nm. The size distribution shifted from a broad peak to a uniform decreased peak, suggesting that the cross-linked networks have transformed into dispersed small aggregates. When the irradiated solution was aged for 12 h at room temperature, the DLS curve exhibited a similar distribution as that for the solution of the initial **6** and heparin composites, indicating that the multi-component assemblies had converted back to the initial cross-linked networks. Additionally, the composite solutions of heparin with **MPY** and reference compound $\mathbf{R}_1$ displayed uniform distributions with averages sizes at 165 and 335 nm, respectively (Figure 7i, black and red lines), corresponding to small aggregates formed. Furthermore, the DLS curve of the heparin and $\mathbf{R}_2$ composites solution exhibited no significant changes when the solution was exposed to 420 nm light for 4 h, suggesting the polymer morphology was retained (Figure 7i, blue and pink lines). The results obtained by DLS experiments were fully consistent with the TEM analysis, which further confirmed the electrostatic-interactions-induced supramolecular aggregation and control of the secondary aggregation process. In fact, these motorized metallacycles act as a kind of photo-responsive supramolecular "glue" for dynamic cross-linking in the networks.

CONCLUSION

In summary, we have successfully organized photo-responsive molecular motors into different sized discrete metallacycles by

https://dx.doi.org/10.1021/jacs.0c11752
J. Am. Chem. Soc. 2021, 143, 442−452

coordinating molecular-motor-based electron-rich donor **MPY** with different electron-deficient di-Pt(II) acceptors. The structures of the metallacycles were confirmed by multi-nuclear NMR (^{1}H and ^{31}P), ESI-TOF-MS, and 2D NMR, and the specific sizes of three different metallacycles were supported by theoretical simulations. UV−vis and NMR spectroscopy revealed that the molecular motor units located on the metallacycles could undergo efficient photo- and thermal isomerization steps similar to free molecular motor ligands. Upon coordination of the pyridine ligands to Pt, the absorption maxima of the motor units exhibited red-shifts, allowing these metallacycle motors to be driven by visible light. Kinetic studies for the thermal isomerization steps of metallacycles illustrated that the coordination of the free ligand donors and di-Pt(II) acceptors had no influence on the isomerization processes or the rotation speed of molecular motors. Experimental CD data, supported by calculations, confirmed that the helicity inversions of the molecular motors were preserved in the discrete metallacycles during the photo- and thermal isomerization processes. These findings have demonstrated that the coordination-driven self-assembly provides a facile approach to organize several single molecular motors and reveal a potential design strategy to implement collective motions. Toward such a goal, the metallacycles were employed as building blocks in a subsequent supramolecular aggregation process with heparin, exploiting multiple electrostatic interactions to construct a multi-component hierarchical system. SEM, TEM, and DLS analysis revealed that the photo- and thermal-responsive molecular motor units enabled selectively manipulation of the secondary aggregation process, i.e., the formation of cross-linked aggregates of metallacycles and heparin, realizing reversible morphology transformations between cross-linked networks and primary supramolecular architectures. These visible-light-responsive metallacycles offer prospects as novel building blocks to construct biomimetic hierarchical self-assembled systems and to fulfill functions reminiscent of dynamic polypeptide and protein assemblies.

■ ASSOCIATED CONTENT

Supporting Information

The Supporting Information is available free of charge at https://pubs.acs.org/doi/10.1021/jacs.0c11752.

Synthesis, characterization, NMR spectra, crystallography, and other experimental details (PDF)

X-ray crystallography data for racemic **MPY** (CIF)

X-ray crystallography data for (*S*,*P*)-**MPY** (CIF)

X-ray crystallography data for (*R*,*M*)-**MPY** (CIF)

■ AUTHOR INFORMATION

Corresponding Authors

Ben L. Feringa − *Key Laboratory for Advanced Materials and Joint International Research Laboratory of Precision Chemistry and Molecular Engineering, Feringa Nobel Prize Scientist Joint Research Center, Frontiers Science Center for Materiobiology and Dynamic Chemistry, Institute of Fine Chemicals, School of Chemistry and Molecular Engineering, East China University of Science and Technology, Shanghai 200237, China; Center for System Chemistry, Stratingh Institute for Chemistry, University of Groningen, 9747 AG Groningen, The Netherlands;* orcid.org/0000-0003-0588-8435; Email: b.l.feringa@rug.nl

Hai-Bo Yang − *Shanghai Key Laboratory of Green Chemistry and Chemical Processes, School of Chemistry and Molecular Engineering, East China Normal University, Shanghai 200062, China;* orcid.org/0000-0003-4926-1618; Email: hbyang@chem.ecnu.edu.cn

Da-Hui Qu − *Key Laboratory for Advanced Materials and Joint International Research Laboratory of Precision Chemistry and Molecular Engineering, Feringa Nobel Prize Scientist Joint Research Center, Frontiers Science Center for Materiobiology and Dynamic Chemistry, Institute of Fine Chemicals, School of Chemistry and Molecular Engineering, East China University of Science and Technology, Shanghai 200237, China;* orcid.org/0000-0002-2039-3564; Email: dahui_qu@ecust.edu.cn

Authors

Zhao-Tao Shi − *Key Laboratory for Advanced Materials and Joint International Research Laboratory of Precision Chemistry and Molecular Engineering, Feringa Nobel Prize Scientist Joint Research Center, Frontiers Science Center for Materiobiology and Dynamic Chemistry, Institute of Fine Chemicals, School of Chemistry and Molecular Engineering, East China University of Science and Technology, Shanghai 200237, China*

Yi-Xiong Hu − *Shanghai Key Laboratory of Green Chemistry and Chemical Processes, School of Chemistry and Molecular Engineering, East China Normal University, Shanghai 200062, China*

Zhubin Hu − *State Key Laboratory of Precision Spectroscopy, East China Normal University, Shanghai 200062, China*

Qi Zhang − *Key Laboratory for Advanced Materials and Joint International Research Laboratory of Precision Chemistry and Molecular Engineering, Feringa Nobel Prize Scientist Joint Research Center, Frontiers Science Center for Materiobiology and Dynamic Chemistry, Institute of Fine Chemicals, School of Chemistry and Molecular Engineering, East China University of Science and Technology, Shanghai 200237, China; Center for System Chemistry, Stratingh Institute for Chemistry, University of Groningen, 9747 AG Groningen, The Netherlands*

Shao-Yu Chen − *Key Laboratory for Advanced Materials and Joint International Research Laboratory of Precision Chemistry and Molecular Engineering, Feringa Nobel Prize Scientist Joint Research Center, Frontiers Science Center for Materiobiology and Dynamic Chemistry, Institute of Fine Chemicals, School of Chemistry and Molecular Engineering, East China University of Science and Technology, Shanghai 200237, China; Center for System Chemistry, Stratingh Institute for Chemistry, University of Groningen, 9747 AG Groningen, The Netherlands*

Meng Chen − *Key Laboratory for Advanced Materials and Joint International Research Laboratory of Precision Chemistry and Molecular Engineering, Feringa Nobel Prize Scientist Joint Research Center, Frontiers Science Center for Materiobiology and Dynamic Chemistry, Institute of Fine Chemicals, School of Chemistry and Molecular Engineering, East China University of Science and Technology, Shanghai 200237, China*

Jing-Jing Yu − *Key Laboratory for Advanced Materials and Joint International Research Laboratory of Precision Chemistry and Molecular Engineering, Feringa Nobel Prize Scientist Joint Research Center, Frontiers Science Center for Materiobiology and Dynamic Chemistry, Institute of Fine Chemicals, School of Chemistry and Molecular Engineering,*

https://dx.doi.org/10.1021/jacs.0c11752
J. Am. Chem. Soc. 2021, 143, 442−452

East China University of Science and Technology, Shanghai 200237, China

Guang-Qiang Yin − *College of Chemistry and Environmental Engineering, Shenzhen University, Shenzhen 518055, China*

Haitao Sun − *State Key Laboratory of Precision Spectroscopy, East China Normal University, Shanghai 200062, China;* orcid.org/0000-0003-1471-8876

Lin Xu − *Shanghai Key Laboratory of Green Chemistry and Chemical Processes, School of Chemistry and Molecular Engineering, East China Normal University, Shanghai 200062, China*

Xiaopeng Li − *College of Chemistry and Environmental Engineering, Shenzhen University, Shenzhen 518055, China;* orcid.org/0000-0001-9655-9551

He Tian − *Key Laboratory for Advanced Materials and Joint International Research Laboratory of Precision Chemistry and Molecular Engineering, Feringa Nobel Prize Scientist Joint Research Center, Frontiers Science Center for Materiobiology and Dynamic Chemistry, Institute of Fine Chemicals, School of Chemistry and Molecular Engineering, East China University of Science and Technology, Shanghai 200237, China;* orcid.org/0000-0003-3547-7485

Complete contact information is available at: https://pubs.acs.org/10.1021/jacs.0c11752

Author Contributions

†Z.-T.S. and Y.-X.H. contributed equally.

Notes

The authors declare no competing financial interest.

■ ACKNOWLEDGMENTS

This work was supported by the National Natural Science Foundation of China (grants 22025503, 21790361, 21871084, and 21672060), Shanghai Municipal Science and Technology Major Project (grant 2018SHZDZX03), the Fundamental Research Funds for the Central Universities, the Programme of Introducing Talents of Discipline to Universities (grant B16017), Program of Shanghai Academic/Technology Research Leader (19XD1421100), and the Shanghai Science and Technology Committee (grant 17520750100). B.L.F. acknowledges financial support of The Netherlands Ministry of Education, Culture and Science (Gravitation program 024.601035) and the European Research Council (ERC, advanced grant no. 694345 to B.L.F.). We thank the Research Center of Analysis and Test of East China University of Science and Technology for help on the characterization.

■ REFERENCES

(1) Berg, J. M.; Tymoczko, J. L.; Stryer, L. *Biochemsitry*, 5th ed.; W.H. Freeman: New York, 2003; Chap. 34.

(2) Sluysmans, D.; Stoddart, J. F. Growing community of artificial molecular machinists. *Proc. Natl. Acad. Sci. U. S. A.* **2018**, *115*, 9359−9361.

(3) Kinbara, K.; Aida, T. Toward intelligent molecular machines: directed motions of biological and artificial molecules and assemblies. *Chem. Rev.* **2005**, *105*, 1377−1400.

(4) van Leeuwen, T.; Lubbe, A. S.; Štacko, P.; Wezenberg, S. J.; Feringa, B. L. Dynamic control of function by light-driven molecular motors. *Nat. Rev. Chem.* **2017**, *1*, 0096.

(5) Dietrich-Buchecker, C.; Jimenez-Molero, M. C.; Sartor, V.; Sauvage, J. P. Rotaxanes and catenanes as prototypes of molecular machines and motors. *Pure Appl. Chem.* **2003**, *75*, 1383−1393.

(6) Erbas-Cakmak, S.; Leigh, D. A.; McTernan, C. T.; Nussbaumer, A. L. Artificial Molecular Machines. *Chem. Rev.* **2015**, *115*, 10081−10206.

(7) Kassem, S.; van Leeuwen, T.; Lubbe, A. S.; Wilson, M. R.; Feringa, B. L.; Leigh, D. A. Artificial molecular motors. *Chem. Soc. Rev.* **2017**, *46*, 2592−2621.

(8) Lancia, F.; Ryabchun, A.; Katsonis, N. Life-like motion driven by artificial molecular machines. *Nat. Rev. Chem.* **2019**, *3*, 536.

(9) Bruns, C. J.; Stoddart, J. F. *The nature of the mechanical bond: from molecules to machines*; Wiley-VCH: Weinheim, 2016.

(10) Balzani, V.; Credi, A.; Venturi, M. *Molecular devices and machines: concepts and perspectives for the nanoworld*, 2nd ed.; Wiley-VCH: Weinheim, 2008.

(11) Browne, W. R.; Feringa, B. L. Making molecular machines work. *Nat. Nanotechnol.* **2006**, *1*, 25−35.

(12) Zhang, Q.; Qu, D. H.; Tian, H.; Feringa, B. L. Bottom-up: can supramolecular tools deliver responsiveness from molecular motors to macroscopic materials? *Matter* **2020**, *3*, 355−370.

(13) Astumian, R. D. How molecular motors work-insights from the molecular machinist's toolbox: the Nobel prize in Chemistry 2016. *Chem. Sci.* **2017**, *8*, 840−845.

(14) Corra, S.; Curcio, M.; Baroncini, M.; Silvi, S.; Credi, A. Photoactivated artificial molecular machines that can perform tasks. *Adv. Mater.* **2020**, *32*, 1906064.

(15) Coskun, A.; Banaszak, M.; Astumian, R. D.; Stoddart, J. F.; Grzybowski, B. A. Great expectations: Can artificial molecular machines deliver on their promise? *Chem. Soc. Rev.* **2012**, *41*, 19−30.

(16) Sagara, Y.; Karman, M.; Verde-Sesto, E.; Matsuo, K.; Kim, Y.; Tamaoki, N.; Weder, C. Rotaxanes as mechanochromic fluorescent force transducers in polymers. *J. Am. Chem. Soc.* **2018**, *140*, 1584−1587.

(17) van Dijk, L.; Tilby, M. J.; Szpera, R.; Smith, O. A.; Bunce, H. A.; Fletcher, S. P. Molecular machines for catalysis. *Nat. Rev. Chem.* **2018**, *2*, 0117.

(18) Ragazzon, G.; Baroncini, M.; Silvi, S.; Venturi, M.; Credi, A. Light-powered autonomous and directional molecular motion of a dissipative self-assembling system. *Nat. Nanotechnol.* **2015**, *10*, 70−75.

(19) Chen, S.; Wang, Y.; Nie, T.; Bao, C.; Wang, C.; Xu, T.; Lin, Q.; Qu, D. H.; Gong, X.; Yang, Y.; Zhu, L.; Tian, H. An Artificial molecular shuttle operates in lipid bilayers for ion transport. *J. Am. Chem. Soc.* **2018**, *140*, 17992−17998.

(20) Zhang, Q.; Rao, S. J.; Xie, T.; Li, X.; Xu, T. Y.; Li, D. W.; Qu, D. H.; Long, Y. T.; Tian, H. Muscle-like artificial molecular actuators for Nnanoparticles. *Chem* **2018**, *4*, 2670−2684.

(21) Credi, A. A molecular cable car for transmembrane ion transport. *Angew. Chem., Int. Ed.* **2019**, *58*, 4108−4110.

(22) Garcia-Lopez, V.; Liu, D.; Tour, J. M. Light-activated organic molecular motors and their applications. *Chem. Rev.* **2020**, *120*, 79−124.

(23) Dattler, D.; Fuks, G.; Heiser, J.; Moulin, E.; Perrot, A.; Yao, X.; Giuseppone, N. Design of collective motions from synthetic molecular switches, rotors, and motors. *Chem. Rev.* **2020**, *120*, 310−433.

(24) Baroncini, M.; Silvi, S.; Credi, A. Photo- and redox-driven artificial molecular motors. *Chem. Rev.* **2020**, *120*, 200−268.

(25) Roke, D.; Wezenberg, S. J.; Feringa, B. L. Molecular rotary motors: Unidirectional motion around double bonds. *Proc. Natl. Acad. Sci. U. S. A.* **2018**, *115*, 9423−9431.

(26) Petermayer, C.; Dube, H. Indigoid photoswitches: visible light responsive molecular tools. *Acc. Chem. Res.* **2018**, *51*, 1153−1163.

(27) Maynard, J. R.; Goldup, S. M. Strategies for the Synthesis of enantiopure mechanically chiral molecules. *Chem* **2020**, *6*, 1914−1932.

(28) Ube, H.; Yamada, R.; Ishida, J. I.; Sato, H.; Shiro, M.; Shionoya, M. A circularly arranged sextuple triptycene gear molecule. *J. Am. Chem. Soc.* **2017**, *139*, 16470−16473.

(29) Ube, H.; Yasuda, Y.; Sato, H.; Shionoya, M. Metal-centred azaphosphatriptycene gear with a photo-and thermally driven mechanical switching function based on coordination isomerism. *Nat. Commun.* **2017**, *8*, 14296.

(30) Koumura, N.; Zijlstra, R. W.; van Delden, R. A.; Harada, N.; Feringa, B. L. Light-driven monodirectional molecular rotor. *Nature* **1999**, *401*, 152−155.

(31) Koumura, N.; Geertsema, E. M.; van Gelder, M. B.; Meetsma, A.; Feringa, B. L. Second generation light-driven molecular motors. Unidirectional rotation controlled by a single stereogenic center with near-perfect photoequilibria and acceleration of the speed of rotation by structural modification. *J. Am. Chem. Soc.* **2002**, *124*, 5037−5051.
(32) Feringa, B. L. The art of building small: from molecular switches to motors (Nobel lecture). *Angew. Chem., Int. Ed.* **2017**, *56*, 11060−11078.
(33) Wezenberg, S. J.; Feringa, B. L. Photocontrol of anion binding affinity to a bis-urea receptor derived from stiff-stilbene. *Org. Lett.* **2017**, *19*, 324−327.
(34) Wang, J.; Feringa, B. L. Dynamic control of chiral space in a catalytic asymmetric reaction using a molecular motor. *Science* **2011**, *331*, 1429−1432.
(35) Dorel, R.; Feringa, B. L. Stereodivergent anion binding catalysis with molecular motors. *Angew. Chem.* **2020**, *132*, 795−799.
(36) Pijper, D.; Feringa, B. L. Molecular transmission: controlling the twist sense of a helical polymer with a single light-driven molecular motor. *Angew. Chem., Int. Ed.* **2007**, *46*, 3693−3696.
(37) Zhao, D.; van Leeuwen, T.; Cheng, J.; Feringa, B. L. Dynamic control of chirality and self-assembly of double-stranded helicates with light. *Nat. Chem.* **2017**, *9*, 250.
(38) Eelkema, R.; Pollard, M. M.; Vicario, J.; Katsonis, N.; Ramon, B. S.; Bastiaansen, C. W. M.; Broer, D. J.; Feringa, B. L. Nanomotor rotates microscale objects. *Nature* **2006**, *440*, 163−163.
(39) Orlova, T.; Lancia, F.; Loussert, C.; Iamsaard, S.; Katsonis, N.; Brasselet, E. Revolving supramolecular chiral structures powered by light in nanomotor-doped liquid crystals. *Nat. Nanotechnol.* **2018**, *13*, 304−308.
(40) Chen, K. Y.; Ivashenko, O.; Carroll, G. T.; Robertus, J.; Kistemaker, J. C.; London, G.; Browne, W. R.; Rudolf, P.; Feringa, B. L. Control of surface wettability using tripodal light-activated molecular motors. *J. Am. Chem. Soc.* **2014**, *136*, 3219−3224.
(41) Pollard, M. M.; Lubomska, M.; Rudolf, P.; Feringa, B. L. Controlled rotary motion in a monolayer of molecular motors. *Angew. Chem.* **2007**, *119*, 1300−1302.
(42) Carroll, G. T.; Pollard, M. M.; van Delden, R.; Feringa, B. L. Controlled rotary motion of light-driven molecular motors assembled on a gold film. *Chem. Sci.* **2010**, *1*, 97−101.
(43) Li, Q.; Fuks, G.; Moulin, E.; Maaloum, M.; Rawiso, M.; Kulic, I.; Foy, J. T.; Giuseppone, N. Macroscopic ccontraction of a gel induced by the integrated motion of light-driven molecular motors. *Nat. Nanotechnol.* **2015**, *10*, 161−165.
(44) Foy, J. T.; Li, Q.; Goujon, A.; Colard-Itté, J. R.; Fuks, G.; Moulin, E.; Schiffmann, O.; Dattler, D.; Funeriu, D. P.; Giuseppone, N. Dual-light control of nanomachines that integrate motor and modulator subunits. *Nat. Nanotechnol.* **2017**, *12*, 540−545.
(45) Chen, J.; Leung, F. K.-C.; Stuart, M. C. A.; Kajitani, T.; Fukushima, T.; van der Giessen, E.; Feringa, B. L. Artificial muscle-like function from hierarchical supramolecular assembly of photoresponsive molecular motors. *Nat. Chem.* **2018**, *10*, 132−138.
(46) Danowski, W.; van Leeuwen, T.; Abdolahzadeh, S.; Roke, D.; Browne, W. R.; Wezenberg, S. J.; Feringa, B. L. Unidirectional rotary motion in a metal-organic framework. *Nat. Nanotechnol.* **2019**, *14*, 488−494.
(47) Danowski, W.; Castiglioni, F.; Sardjan, A. S.; Krause, S.; Pfeifer, L.; Roke, D.; Comotti, A.; Browne, W. R.; Feringa, B. L. Visible-light-driven rotation of molecular motors in a dual-function metal-organic framework enabled by energy transfer. *J. Am. Chem. Soc.* **2020**, *142*, 9048−9056.
(48) Chakrabarty, R.; Mukherjee, P. S.; Stang, P. J. Supramolecular coordination: self-assembly of finite two- and three-dimensional ensembles. *Chem. Rev.* **2011**, *111*, 6810−6918.
(49) Fujita, M.; Tominaga, M.; Hori, A.; Therrien, B. Coordination assemblies from a Pd(II)-cornered square complex. *Acc. Chem. Res.* **2005**, *38*, 369−378.
(50) Chakraborty, S.; Newkome, G. R. Terpyridine-based metallosupramolecular constructs: tailored monomers to precise 2D-motifs and 3D-metallocages. *Chem. Soc. Rev.* **2018**, *47*, 3991−4016.
(51) Pesce, L.; Perego, C.; Grommet, A. B.; Klajn, R.; Pavan, G. M. Molecular factors controlling the isomerization of azobenzenes in the cavity of a flexible coordination cage. *J. Am. Chem. Soc.* **2020**, *142*, 9792−9802.
(52) Yamashina, M.; Tanaka, Y.; Lavendomme, R.; Ronson, T. K.; Pittelkow, M.; Nitschke, J. R. An antiaromatic-walled nanospace. *Nature* **2019**, *574*, 511−515.
(53) Zhang, D.; Ronson, T. K.; Nitschke, J. R. Functional capsules via subcomponent self-assembly. *Acc. Chem. Res.* **2018**, *51*, 2423−2436.
(54) Foster, J. A.; Parker, R. M.; Belenguer, A. M.; Kishi, N.; Sutton, S.; Abell, C.; Nitschke, J. R. Differentially addressable cavities within metal-organic cage-cross-linked polymeric hydrogels. *J. Am. Chem. Soc.* **2015**, *137*, 9722−9729.
(55) Schulte, T. R.; Holstein, J. J.; Schneider, L.; Adam, A.; Haberhauer, G.; Clever, G. H. A new mechanically-Interlocked $[Pd_2L_4]$ cage motif by dimerization of two peptide-based lemniscates. *Angew. Chem., Int. Ed.* **2020**, *59*, 22270.
(56) Schulte, T. R.; Holstein, J. J.; Clever, G. H. Chiral self-discrimination and guest recognition in helicene-based coordination cages. *Angew. Chem., Int. Ed.* **2019**, *58*, 5562−5566.
(57) Li, G.; Zhou, Z.; Yuan, C.; Guo, Z.; Liu, Y.; Zhao, D.; Liu, K.; Zhao, J.; Tan, H.; Yan, X. Trackable supramolecular fusion: cage to cage transformation of tetraphenylethylene-based metalloassemblies. *Angew. Chem., Int. Ed.* **2020**, *59*, 10013−10017.
(58) Li, P.-Z.; Wang, X.-J.; Zhao, Y. L. Click chemistry as a versatile reaction for construction and modification of metal-organic frameworks. *Coord. Chem. Rev.* **2019**, *380*, 484−518.
(59) Hong, C. M.; Bergman, R. G.; Raymond, K. N.; Toste, F. D. Self-assembled tetrahedral hosts as supramolecular catalysts. *Acc. Chem. Res.* **2018**, *51*, 2447−2455.
(60) Oldacre, A. N.; Friedman, A. E.; Cook, T. R. A Self-assembled cofacial cobalt porphyrin prism for oxygen reduction catalysis. *J. Am. Chem. Soc.* **2017**, *139*, 1424−1427.
(61) Chen, L.-J.; Chen, S.; Qin, Y.; Xu, L.; Yin, G.-Q.; Zhu, J.-L.; Zhu, F.-F.; Zheng, W.; Li, X.; Yang, H.-B. Construction of porphyrin-containing metallacycle with improved stability and activity within mesoporous carbon. *J. Am. Chem. Soc.* **2018**, *140*, 5049−5052.
(62) Ueda, Y.; Ito, H.; Fujita, D.; Fujita, M. Permeable self-assembled molecular containers for catalyst isolation enabling two-step cascade reactions. *J. Am. Chem. Soc.* **2017**, *139*, 6090−6093.
(63) Xu, L.; Zhang, D.; Ronson, T.; Nitschke, J. Improved Acid Resistance of a Metal-Organic Cage Enables Cargo Release and Exchange between Hosts. *Angew. Chem., Int. Ed.* **2020**, *59*, 7435−7438.
(64) Han, M.; Michel, R.; He, B.; Chen, Y.-S.; Stalke, D.; John, M.; Clever, G. H. Light-triggered guest uptake and release by a photochromic coordination cage. *Angew. Chem., Int. Ed.* **2013**, *52*, 1319−1323.
(65) Howlader, P.; Mondal, B.; Purba, P. C.; Zangrando, E.; Mukherjee, P. S. Self-assembled Pd(II) barrels as containers for transient merocyanine form and reverse thermochromism of spiropyran. *J. Am. Chem. Soc.* **2018**, *140*, 7952−7960.
(66) Yoshizawa, M.; Catti, L. Bent anthracene dimers as versatile building blocks for supramolecular capsules. *Acc. Chem. Res.* **2019**, *52*, 2392−2404.
(67) Canton, M.; Grommet, A. B.; Pesce, L.; Gemen, J.; Li, S.; Diskin-Posner, Y.; Credi, A.; Pavan, G. M.; Andréasson, J.; Klajn, R. Improving fatigue resistance of dihydropyrene by encapsulation within a coordination cage. *J. Am. Chem. Soc.* **2020**, *142*, 14557−14565.
(68) Hu, Y.-X.; Hao, X.; Xu, L.; Xie, X.; Xiong, B.; Hu, Z.; Sun, H.; Yin, G.-Q.; Li, X.; Peng, H.; Yang, H.-B. Construction of supramolecular liquid-crystalline metallacycles for holographic storage of colored images. *J. Am. Chem. Soc.* **2020**, *142*, 6285−6294.
(69) Kawano, S.; Ishida, Y.; Tanaka, K. Columnar liquid-crystalline metallomacrocycles. *J. Am. Chem. Soc.* **2015**, *137*, 2295−2302.
(70) Chen, L.; Chen, C.; Sun, Y.; Lu, S.; Huo, H.; Tan, T.; Li, A.; Li, X.; Ungar, G.; Liu, F.; Zhang, M. Luminescent metallacycle-cored liquid crystals induced by metal coordination. *Angew. Chem.* **2020**, *132*, 10229−10236.

https://dx.doi.org/10.1021/jacs.0c11752
J. Am. Chem. Soc. 2021, 143, 442−452

(71) Uchida, J.; Yoshio, M.; Sato, S.; Yokoyama, H.; Fujita, M.; Kato, T. Self-assembly of giant spherical liquid-crystalline complexes and formation of nanostructured dynamic gels exhibiting self-healing properties. *Angew. Chem., Int. Ed.* **2017**, *56*, 14085−14089.
(72) Pitto-Barry, A.; Barry, N. P. E.; Russo, V.; Heinrich, B.; Donnio, B.; Therrien, B.; Deschenaux, R. Designing supramolecular liquid-crystalline hybrids from pyrenyl-containing dendrimers and arene ruthenium metallacycles. *J. Am. Chem. Soc.* **2014**, *136*, 17616−17625.
(73) Wang, J.; He, C.; Wu, P. Y.; Wang, J.; Duan, C. Y. An amide-containing metal-organic tetrahedron responding to a spin-trapping reaction in a fluorescent enhancement manner for biological imaging of NO in living cells. *J. Am. Chem. Soc.* **2011**, *133*, 12402−12405.
(74) Yamashina, M.; Sartin, M. M.; Sei, Y.; Akita, M.; Takeuchi, S.; Tahara, T.; Yoshizawa, M. Preparation of highly fluorescent host-guest complexes with tunable color upon encapsulation. *J. Am. Chem. Soc.* **2015**, *137*, 9266−9269.
(75) Acharyya, K.; Bhattacharyya, S.; Sepehrpour, H.; Chakraborty, S.; Lu, S.; Shi, B.; Li, X.; Mukherjee, P. S.; Stang, P. J. Self-assembled fluorescent Pt (II) metallacycles as artificial light-harvesting systems. *J. Am. Chem. Soc.* **2019**, *141*, 14565−14569.
(76) Zhu, H.; Li, Q.; Shi, B.; Xing, H.; Sun, Y.; Lu, S.; Shangguan, L.; Li, X.; Huang, F.; Stang, P. J. Formation of planar chiral platinum triangles via pillar[5]arene for circularly polarized luminescence. *J. Am. Chem. Soc.* **2020**, *142*, 17340−17345.
(77) Qin, Y.; Chen, L.-J.; Dong, F.; Jiang, S.-T.; Yin, G.-Q.; Li, X.; Tian, Y.; Yang, H.-B. Light-controlled generation of singlet oxygen within a discrete dual-stage metallacycle for cancer therapy. *J. Am. Chem. Soc.* **2019**, *141*, 8943−8950.
(78) Zhou, J.; Zhang, Y.; Yu, G.; Crawley, M. R.; Fulong, C. R. P.; Friedman, A. E.; Sengupta, S.; Sun, J.; Li, Q.; Huang, F.; Cook, T. R. Highly emissive self-assembled BODIPY-platinum supramolecular triangles. *J. Am. Chem. Soc.* **2018**, *140*, 7730−7736.
(79) Gao, S.; Yan, X.; Xie, G.; Zhu, M.; Ju, X.; Stang, P. J.; Tian, Y.; Niu, Z. Membrane intercalation-enhanced photodynamic inactivation of bacteria by a metallacycle and TAT-decorated virus coat protein. *Proc. Natl. Acad. Sci. U. S. A.* **2019**, *116*, 23437−23443.
(80) Gemen, J.; Ahrens, J.; Shimon, L. J.; Klajn, R. Modulating the optical properties of BODIPY dyes by noncovalent dimerization within a flexible coordination cage. *J. Am. Chem. Soc.* **2020**, *142*, 17721−17729.
(81) Wang, D.; Wu, H.; Lim, W. Q.; Phua, S. Z. F.; Xu, P.; Chen, Q.; Guo, Z.; Zhao, Y. L. A mesoporous nanoenzyme derived from metal-organic frameworks with endogenous oxygen generation to alleviate tumor hypoxia for significantly enhanced photodynamic therapy. *Adv. Mater.* **2019**, *31*, 1901893.
(82) Wang, W.; Wang, Y.-X.; Yang, H.-B. Supramolecular transformations within discrete coordination-driven supramolecular architectures. *Chem. Soc. Rev.* **2016**, *45*, 2656−2693.
(83) McConnell, A. J.; Wood, C. S.; Neelakandan, P. P.; Nitschke, J. R. Stimuli-responsive metal-ligand assemblies. *Chem. Rev.* **2015**, *115*, 7729−7793.
(84) Chen, L.-J.; Yang, H.-B. Construction of stimuli-responsive functional materials via hierarchical self-assembly involving coordination interactions. *Acc. Chem. Res.* **2018**, *51*, 2699−2710.
(85) Yan, X.; Xu, J.-F.; Cook, T. R.; Huang, F.; Yang, Q.-Z.; Tung, C.-H.; Stang, P. J. Photoinduced transformations of stiff-stilbene based discrete metallacycles to metallosupramolecular polymers. *Proc. Natl. Acad. Sci. U. S. A.* **2014**, *111*, 8717−8722.
(86) Yang, H.-B.; Ghosh, K.; Arif, A. M.; Stang, P. J. The synthesis of new 60° organometallic subunits and self-assembly of three-dimensional M_3L_2 trigonal-bipyramidal cages. *J. Org. Chem.* **2006**, *71*, 9464−9469.
(87) Yang, H.-B.; Ghosh, K.; Zhao, Y.; Northrop, B. H.; Lyndon, M. M.; Muddiman, D. C.; White, H. S.; Stang, P. J. A new family of multiferrocene complexes with enhanced control of structure and stoichiometry via coordination-driven self-assembly and their electrochemistry. *J. Am. Chem. Soc.* **2008**, *130*, 839−841.
(88) Manna, J.; Kuehl, C. J.; Whiteford, J. A.; Stang, P. J.; Muddiman, D. C.; Hofstadler, S. A.; Smith, R. D. Nanoscale tectonics: self-assembly, characterization, and chemistry of a novel class of organoplatinum square macrocycles. *J. Am. Chem. Soc.* **1997**, *119*, 11611−11619.
(89) Yu, J. J.; Liang, W. J.; Zhang, Q.; Li, M. M.; Qu, D. H. Photo-powered collapse of supramolecular polymers based on an overcrowded alkene switch. *Chem. - Asian J.* **2019**, *14*, 3141−3144.
(90) Bannwarth, C.; Ehlert, S.; Grimme, S. GFN2-xTB-an accurate and broadly parametrized self-consistent tight-binding quantum chemical method with multipole electrostatics and density-dependent dispersion contributions. *J. Chem. Theory Comput.* **2019**, *15*, 1652−1671.
(91) Štacko, P.; Kistemaker, J. C.; Van Leeuwen, T.; Chang, M. C.; Otten, E.; Feringa, B. L. Locked synchronous rotor motion in a molecular motor. *Science* **2017**, *356*, 964−96.
(92) Cnossen, A.; Hou, L.; Pollard, M. M.; Wesenhagen, P. V.; Browne, W. R.; Feringa, B. L. Driving unidirectional molecular rotary motors with visible light by intra-and intermolecular energy transfer from palladium porphyrin. *J. Am. Chem. Soc.* **2012**, *134*, 17613−17619.
(93) Danowski, W.; Castiglioni, F.; Sardjan, A. S.; Krause, S.; Pfeifer, L.; Roke, D.; Comotti, A.; Browne, W. R.; Feringa, B. L. Visible-light-driven rotation of molecular motors in a dual-function metal-organic framework enabled by energy transfer. *J. Am. Chem. Soc.* **2020**, *142*, 9048−9056.
(94) van Leeuwen, T.; Pol, J.; Roke, D.; Wezenberg, S. J.; Feringa, B. L. Visible-light excitation of a molecular motor with an extended aromatic core. *Org. Lett.* **2017**, *19*, 1402−1405.
(95) Wezenberg, S. J.; Chen, K. Y.; Feringa, B. L. Visible-light-driven photoisomerization and increased rotation speed of a molecular motor acting as a ligand in a ruthenium (II) complex. *Angew. Chem., Int. Ed.* **2015**, *54*, 11457−11461.
(96) Pfeifer, L.; Scherübl, M.; Fellert, M.; Danowski, W.; Cheng, J.; Pol, J.; Feringa, B. L. Photoefficient 2nd generation molecular motors responsive to visible light. *Chem. Sci.* **2019**, *10*, 8768−8773.
(97) Chen, L.-J.; Ren, Y.-Y.; Wu, N.-W.; Sun, B.; Ma, J.-Q.; Zhang, L.; Tan, H.; Liu, M.; Li, X.; Yang, H.-B. Hierarchical self-assembly of discrete organoplatinum(II) metallacycles with polysaccharide via electrostatic interactions and their application for heparin detection. *J. Am. Chem. Soc.* **2015**, *137*, 11725−11735.

https://dx.doi.org/10.1021/jacs.0c11752
J. Am. Chem. Soc. 2021, 143, 442−452